Article │ Received 9 March 2025; Accepted 23 July 2025; Published 31 July 2025
https://doi.org/10.55092/ae20250005

Development of an integrated device for processing and detection of micro and nano structures on a miniaturized sphere utilizing atomic force microscopy

Jiqiang Wang[1], Ziwen Kang[2], Yongda Yan[1,2] and Yanquan Geng[1,*]

[1] The State Key Laboratory of Robotics and Systems, Robotics Institute, Harbin Institute of Technology, Harbin 150080, China

[2] Center for Precision Engineering, Harbin Institute of Technology, Harbin 150001, China

* Correspondence author; E-mail: gengyanquan@hit.edu.cn.

Highlights:

- An integrated device is established to machine and measure on microsphere surface.
- The control system and operation software are developed.
- A strategy for center alignment of microsphere and air-bearing spindle is proposed.
- Nanostructures on microsphere is machined and measured.

Abstract: Microspheres, with diameters ranging from tens of microns to several millimeters, find extensive application in precision bearings, optical cameras, and lithography machines due to their unique mechanical and optical properties. Concurrently, the demand for improved dimensional accuracy and enhanced surface quality of these microspheres has significantly increased. As a result, the research focus has increasingly shifted towards micro-nano structuring and high-precision measurement of microspheres. In this study, an integrated device comprising a custom-developed AFM system, a control system, and proprietary software was established to achieve seamless integration of machining and measurement on the surface of microspheres. Moreover, the control system of the device has been established. The computer software is also developed based on the C++ graphical user interface (GUI) application development framework QT software. To achieve the center alignment between the micro-sphere and the air-bearing spindle, a strategy based on the device is proposed. Nanostructures, including square pit structures, triangular structures, and circular structures, are successfully machined and measured on the surface of GDP microspheres. Our findings provide a new approach for machining and measuring micro-nano structures on the surface of micro-target balls used in ICF.

Keywords: integrated device; home-made AFM; miniaturized sphere; nanofabrication; measurement

1. Introduction

With the rapid advancement of nanotechnology, the unique optical, electrical, magnetic, and mechanical properties of nanostructures have emerged due to their size being in the same order of magnitude as the wavelength of light. These properties stem from surface effects, small size effects, and quantum size effects, leading to widespread applications in nano-optics, nano-biosensors, nano-electronics, and other fields. For instance, in Inertial Confinement Fusion (ICF), the study of Rayleigh-Taylor (RT) instability on the surface nanostructure of a small, low-stiffness target ball is crucial for ensuring the success of fusion experiments. Research into RT instability not only facilitates the smooth implementation of ICF experiments but also explores fundamental scientific issues such as the evolution of astrophysical phenomena. Consequently, there has been increasing attention focused on the processing and detection of micro-nano structures on the surface of micro-target balls.

Currently, researchers predominantly employ laser machining and ultra-precision machining techniques to fabricate micro-nano structures on microspheres. For instance, McEachern *et al.* [1] employed laser ablation technology to create 200 micro-pit structures at random positions on the surface of a microsphere, with processing depths ranging from 0.3 to 1 μm and pit radii of approximately 37 μm. However, this method presents challenges in precisely controlling the machining depth. In contrast, Glendinning *et al.* [2] used an excimer laser processing technique to fabricate a nanostructure template and subsequently imprinted a sinusoidal microstructure with a period of 50–70 μm and an amplitude of 0.5–2 μm over a 280 μm × 280 μm area on the microsphere surface. In addition, Carlson *et al.* [3] employed laser ablation to fabricate the intended structural features on the surface of glow-discharge polymer microspheres used for target shooting. Specifically, a sine-wave structure with a peak-to-valley amplitude of 2 μm was machined on one-third of the outer surface of a high-density carbon target ball with a diameter of 2 mm. However, processing a ripple pattern on the inner surface of the 2-mm-diameter target ball through its 1-mm spherical opening proved significantly more challenging. Takeuchi *et al.* [4] developed a computer-aided manufacturing (CAM) system to achieve precise 6-axis control of a non-rotating cutting tool, enabling the accurate machining of complex micro-groove shapes. Using this six-axis ultra-precision machining center, they successfully fabricated a meshed micro-nano structure with groove widths of 30 μm and depths of 15 μm on a microsphere. Wang *et al.* [5] developed a five-axis microforce-controlled cutting system to process dents in various rings on the near-global surface of the target ball. They experimentally investigated the relationships between cutting depth, applied load, and spindle rotation speed, thereby elucidating the micromachining mechanism. AFM tip based nanomachining is also utilized to fabricate nanostructure on a Miniaturized Sphere. Zhao *et al.* [6] enhanced a AFM system by integrating a commercial AFM with a domestically developed precision air-bearing spindle. This improved system enabled the successful machining of nanowire arrays, surface pit structures, and sawtooth structures on the circumference of a microsphere. Moreover, Geng *et al.* [7] integrated a commercial AFM with a two-dimensional high-precision stage, a high-precision air-bearing spindle, and an electric rotary platform to develop a five-axis nanoscale machine tool for fabricating nanostructures on microspheres. Through precise control of the distance between the center of the microsphere and the rotational axis of the AFM system, they successfully fabricated diverse nanostructures, including square pits, circular pits, triangular pits, and ring nanochannels, on three distinct rings of a 1500-micron-diameter microsphere. The nanostructure is currently fabricated on only a limited area of the micro-ball based on the commercial system.

In addition to the processing of nanostructures on the surface of microspheres, accurately detecting these nanostructures is equally critical. Current research has made notable progress in developing methods for the detection of microsphere nanostructures. Küng *et al.* [8] developed a novel 3D touch probe for coordinate measuring machines (CMM) featuring a replaceable small probe element and low measuring force. Zhao *et al.* [9] designed a target pellet surface profilometer based on AFM, specifically tailored to measure the surface geometric parameters of target pellets with diameters ranging from several hundred microns to several millimeters. Chen *et al.* [10] introduced a 3D contour measurement method combining optical measurement and surface reconstruction. Utilizing a three-dimensional mapping algorithm, this method constructs volumetric data of spherical heads from cross-sectional profiles. The proposed method can measure microspheres with diameters ranging from tens of microns to a few millimeters, demonstrating a maximum measurement error of ±0.5 microns. Bartl *et al.* [11,12] proposed a method for reconstructing the absolute morphology of a sphere using a spherical interferometer in conjunction with a splicing technique. This approach employs a two-sided measurement principle and an advanced splicing algorithm to achieve reliable absolute radius determination. Janecki *et al.* [13] designed and constructed a specialized device for the precise positioning of spherical components. This device enables the test element to be rotated at precisely defined angles around two mutually perpendicular axes, thereby scanning the surface along a predetermined path. Lu *et al.* [14] introduced a novel phase-shifting diffraction interference optical path structure for high-precision microsphere topography measurement, and investigated the subaperture stitching technology employed in this system. Zhao *et al.* [15] developed a high-precision method for measuring the radius and sphericity of CMM probe tip microspheres. Two polarization Michelson interferometers (PMIs) are positioned face-to-face on either side of the microsphere under test, which is mounted on a rotating table via an angle deflector capable of deflecting more than ± βmax. Oertel *et al.* [16] proposed and investigated a method that integrates AFM scanning with a stitching algorithm. This approach was implemented on a nanometric machine, and the proposed strategy for microsphere measurement was validated using a ruby sphere with a radius of 150 microns. The method enables the measurement of large radii with high lateral and longitudinal resolution. The average radius was measured with a repeatability of 3.7 nm, while the root mean square (RMS) deviation of residuals after the stitching process was 8.2 nm. Currently, the measurement and the fabrication process on the micro sphere are separate. Furthermore, the aforementioned processes are carried out on a commercial equipment, which has limitations on the measurement and fabrication.

In this study, to achieve the integration of machining and measurement on the surface of microspheres, we developed an integrated device comprising a homemade AFM system, a control system, and proprietary software. Additionally, we proposed an installation method for aligning the rotating center of the microsphere with the air-bearing spindle, effectively addressing the challenge of center alignment during microsphere machining and testing. Using this homemade integrated device, we successfully machined and tested square pit structures, triangular structures, and circular structures on the surface of microspheres, providing a novel solution for machining and measuring micro-nano structures on the surface of micro-target balls used in ICF.

2. Methods

2.1. Comprehensive design of the mechanical structure

Figure 1a shows the 3D model of the homemade AFM device. The home-made atomic force microscope (AFM) adopts a probe-scanning configuration. The comprehensive structure primarily comprises the force sensing system, an XYZ three-dimensional piezoelectric stage, and a visual assistance system. The probe is driven by the scanner to perform XY scanning and Z feedback on the sample surface, thereby detecting the topographical information of the sample. As illustrated in Figure 1b, the force sensing control system consists of probe, laser, position-sensitive detector (PSD), optical lenses, and other components, all mounted on a Z-direction piezoelectric stage. This stage is further fixed on a large-range Z-direction linear sliding platform, enabling coarse motion over a wide range. The incident and reflected light paths of the force sensing system are adjusted using laser and mirror adjustment frames, respectively. Laser light shines on the probe cantilever and is reflected onto a plane mirror, which then directs the light through a convex lens and focuses it onto the PSD. Beneath the probe lies an XY two-dimensional manual displacement table that controls the macroscopic XY motion of the sample. The probe is fixed on the Z-direction piezoelectric stage, forming a closed-loop control system with the force sensing system. The entire setup is installed on an air-floating vibration isolation platform to minimize external vibration interference. During the processing and detection of the microsphere, the force sensing system rotates 90 degrees, as illustrated in Figure 1c. The rotation of the microsphere facilitates its processing and detection. As depicted in Figure 1d, the XY two-dimensional manual displacement table is connected to the high-precision air-bearing spindle via an adapter plate. The needle is mounted on the displacement table, while the microsphere is securely affixed to the needle using adhesive. The spindle then drives the microsphere to rotate stably.

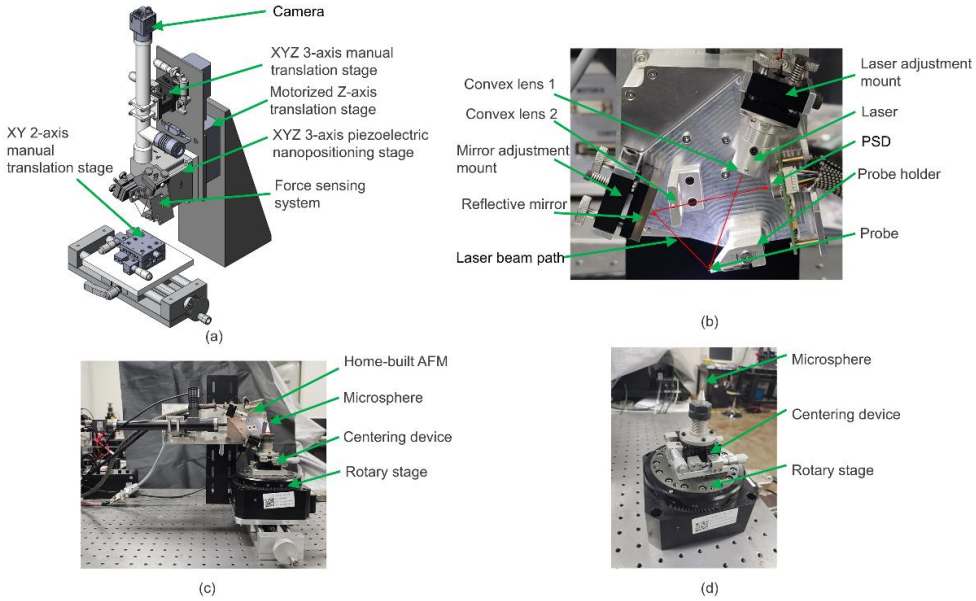

Figure 1. The mechanical structure of the integrated device for processing and detection on a miniaturized sphere. **(a)** The 3D model of the homemade AFM device; **(b)** The image of the force-sensing system; **(c)** The image of the device for measurement and fabrication on a miniaturized sphere; **(d)** Miniaturized sphere holding device.

2.2. The control system

Figure 2 illustrates the diagram of the control system. The host computer is connected to three components: a serial relay, a data acquisition card, and a PID controller. The data acquisition card features 7 analog inputs, 3 analog outputs, and a pulse port. Specifically, the analog inputs include the SUM value signal from the PSD controller, the X difference (Xdiff) signal, the Y difference (Ydiff) signal, the XYZ position signal from the piezoelectric ceramic controller, and the Error signal from the PID controller. The three analog outputs are designated for the XY motion signals to the piezoelectric stage controller and the setpoint signal to the PID controller. The pulse signal, generated by the data acquisition card, is transmitted to the stepper motor controller via a booster module. For normal operation, the stepper motor controller requires three types of signals: pulse, direction, and enable. The direction and enable signals determine the motor's direction and operational status, which are controlled by the serial relay. The serial relay connects to the computer through the RS232 protocol, enabling serial communication and controlling the relay output levels. The pulse signal controls the rotation of the stepper motor.

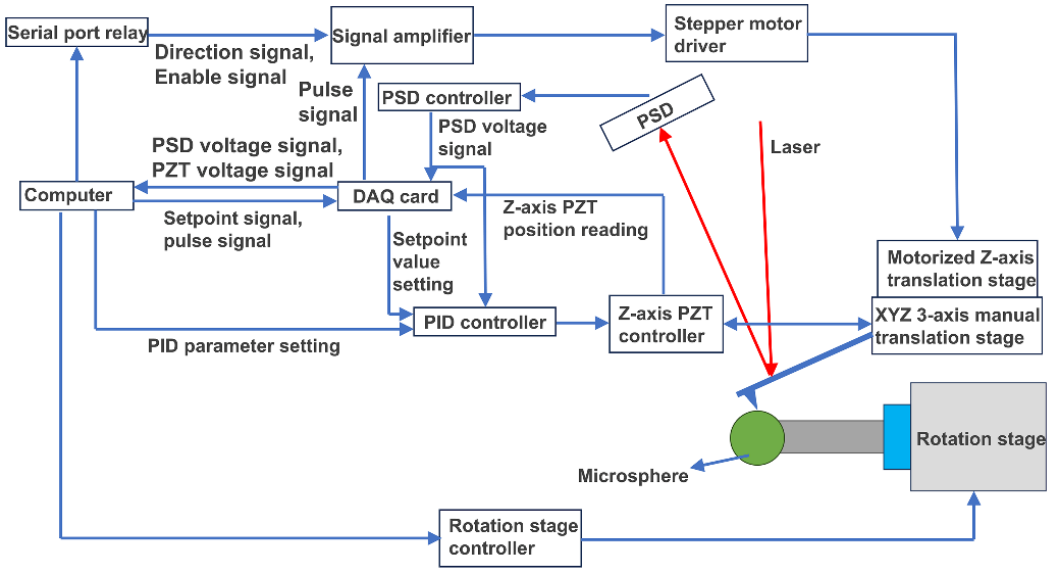

Figure 2. Schematic diagram of the control system for microsphere machining and testing device.

The control system achieves closed-loop control of the analog quantity via a PID controller. The host computer can configure the PID controller parameters, including setpoint, proportional gain, integral gain, and derivative gain, as well as the working mode through serial port instructions. The Ydiff detection voltage signal from the PSD serves as the feedback signal to the PID controller's input port. The output voltage from the PID controller is then applied to the Z-axis analog input port of the piezoelectric ceramic platform, thereby enabling precise motion control along the Z-axis. During scanning, the probe cantilever undergoes deformation, causing the laser spot position to shift. The PSD then generates a Ydiff differential signal, which is fed into the input port of the PID controller. Meanwhile, the setpoint value for the PID controller is provided via an analog voltage signal generated by the data acquisition card. The PID controller adjusts the error between the actual and setpoint values through proportional, integral, and derivative actions, and subsequently adds a bias voltage. This adjusted signal is output to the piezoelectric ceramic controller, which in turn generates a control voltage

to drive the piezoelectric stage. The piezoelectric stage then actuates the probe, forming a closed-loop control system for maintaining consistent force.

For the processing and testing of microspheres, an additional spindle and spindle controller were integrated into our home-made AFM system. The host computer software of the AFM was also enhanced with a function to control the spindle. Specifically, the spindle employed is the ABRS-150MP-M-X50 air-bearing direct-drive turntable manufactured by Aerotech, while the spindle controller is Aerotech' s Soloist controller. The spindle controller is interfaced with the host computer, which sends commands to the spindle controller to regulate the spindle's motion.

2.3. The software

The upper computer software is developed using the C++ graphical user interface (GUI) application development framework Qt software. The AFM software comprises four modules: a common function module, a sphere detection module, a machining module and a local surface detection module.

(1) Common function module

The interface of the common function module is shown in Figure 3. The main functions include Z displacement table control, piezoelectric displacement stage control, engagement of the tip, withdraw of the tip, force curve testing, PID controller parameter setting, real-time display of PSD signal and position signal of piezoelectric displacement stage, *etc*. This module is the basis of the AFM software, and other modules need to be opened through this module.

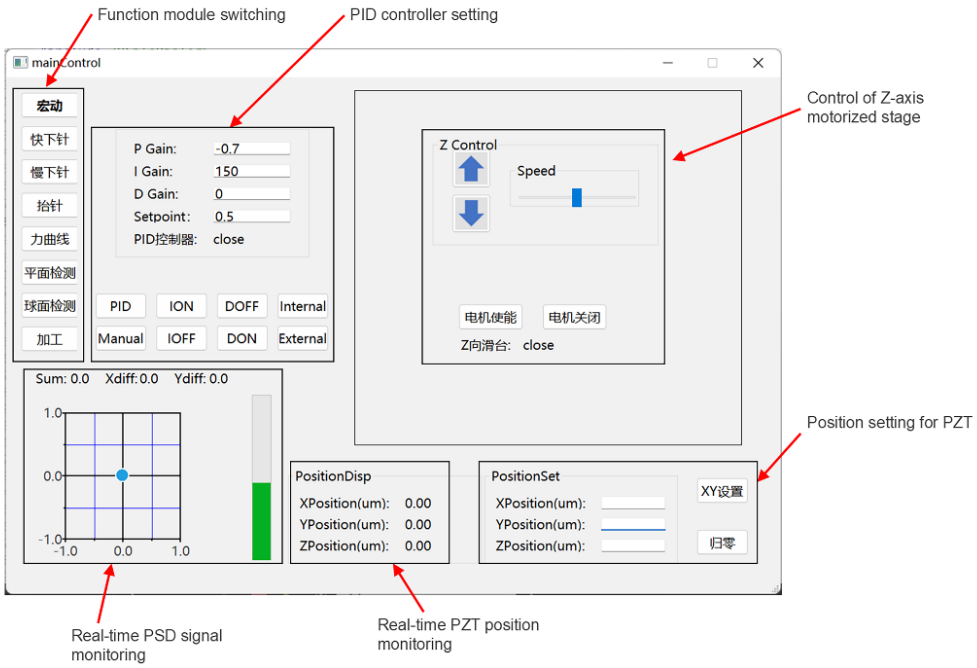

Figure 3. The interface of the common function module.

To enhance the efficiency of the tip engagement process, the automated tip engagement process is divided into two stages: rapid engagement and precise engagement. The workflow diagram for these stages is illustrated in Figure 4. In the first stage, the piezoelectric stage extends by 60 nm per cycle. After each extension, the system checks if the Y-direction differential signal (Ydiff) voltage from the PSD has reached the setpoint value. This process repeats up to 100 cycles. If the piezoelectric stage has

not contracted to 6 μm after these cycles, the electric slide will retract by 5 μm and continue cycling until the differential signal reaches the setpoint value. Figure 4a shows the flowchart for the rapid engagement, where the tip engagement is 5 μm/s. In the second stage, the piezoelectric stage extends by 3 nm per cycle, allowing the Ydiff signal to approach the setpoint value more accurately at the end of engagement process. The tip engagement speed during this stage is reduced to 0.2 μm/s. Following the completion of the second stage, the PID closed-loop control mode is automatically activated.

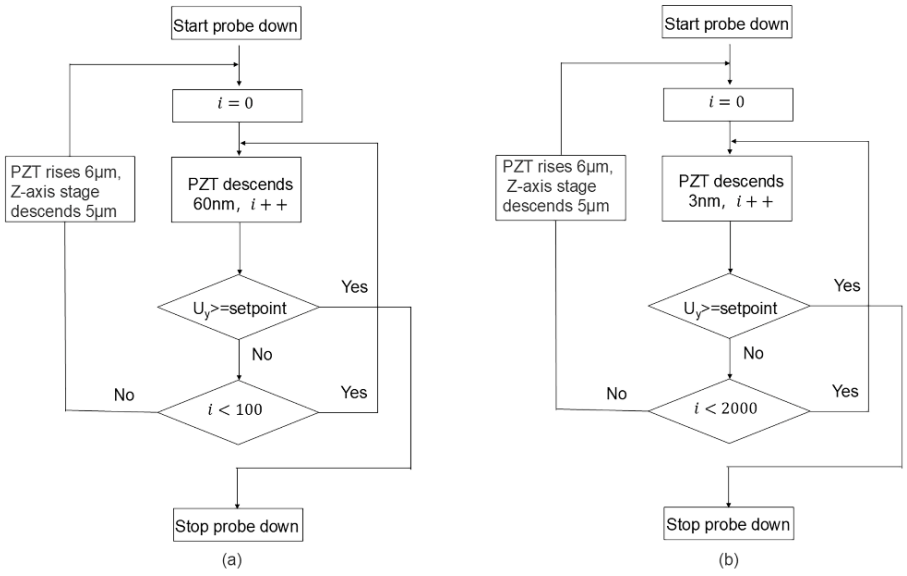

Figure 4. The workflow diagram for engagement process: **(a)** Rapid engagement; **(b)** Precise engagement.

(2) Miniaturized sphere detection module

The interface of the spherical detection module is illustrated in Figure 5. Its primary functions encompass topographical detection, real-time display of the sphere contour, turntable control, computation of eccentric point position, roundness evaluation, and storage of detection data. The software can generate a real-time circular trace image based on the detection data, calculate the radial coordinates using the detected Z-direction piezoelectric ceramic position, determine the angular coordinates by integrating the angular velocity and rotation time, and connect the data points to outline the sphere contour. The software directly computes the eccentric position of the target sphere and its roundness after the measurement. The eccentric position is determined using the least squares method. The computational process within the software proceeds as follows.

Determine the centroid of all data points using the following equation,

$$\bar{x} = \frac{1}{n}\sum_{i=1}^{n} x_i, \quad \bar{y} = \frac{1}{n}\sum_{i=1}^{n} y_i \tag{1}$$

To address the least squares problem, we construct the following matrices and vectors,

$$u_i = x_i - \bar{x}, \quad v_i = y_i - \bar{y} \tag{2}$$

$$S_u = \sum_{i=1}^{n} u_i^2, \quad S_v = \sum_{i=1}^{n} v_i^2, \quad S_{uv} = \sum_{i=1}^{n} u_i v_i \tag{3}$$

$$S_{uuu} = \sum_{i=1}^{n} u_i^3, \quad S_{vvv} = \sum_{i=1}^{n} v_i^3 \tag{4}$$

$$S_{uuv} = \sum_{i=1}^{n} u_i^2 v_i, \quad S_{uvv} = \sum_{i=1}^{n} u_i v_i^2 \tag{5}$$

Subsequently, solve the system of linear equations,

$$\begin{pmatrix} S_u & S_{uv} \\ S_{uv} & S_v \end{pmatrix} \begin{pmatrix} a \\ b \end{pmatrix} = \frac{1}{2} \begin{pmatrix} S_{uuu}+S_{uvv} \\ S_{vvv}+S_{uuv} \end{pmatrix} \tag{6}$$

$$a = \frac{S_{vvv}+S_{uuv}}{2(S_u S_v - S_{uv}^2)}, \quad b = \frac{S_{uuu}+S_{uvv}}{2(S_u S_v - S_{uv}^2)} \tag{7}$$

Finally, the central coordinates are determined as follows.

$$(h, k) = (\bar{x} + a, \bar{y} + b) \tag{8}$$

The center of the circle represents the eccentric position of the target ball. Based on this eccentric position, the farthest and nearest distances in the detection data are calculated. The roundness error of the circular trace is then determined by subtracting these distances.

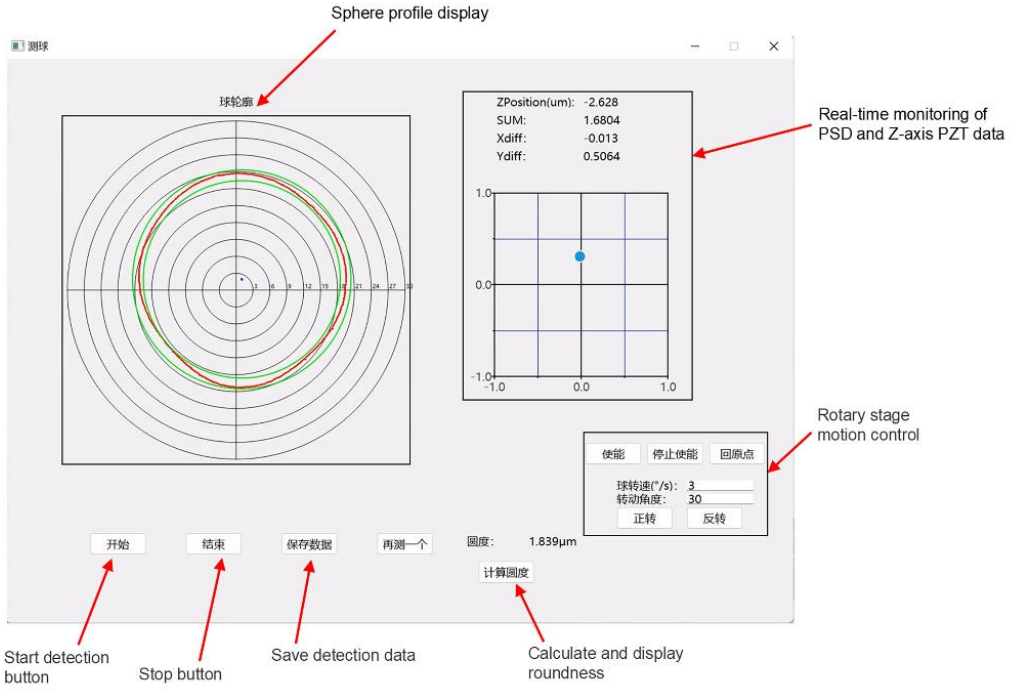

Figure 5. The interface of the spherical detection module.

(3) The machining module

The interface of the machining module, as illustrated in Figure 6, encompasses several key functionalities. These include loading customized processing trajectories, setting parameters such as processing force, shape, and speed, calculating and displaying processing trajectories, monitoring equipment status information, and saving equipment data during processing. The software offers predefined simple shapes, such as nanowires and square pits, which do not require manual calculation

of processing data as it is automatically generated. Additionally, the system supports loading machining data to enable the fabrication of complex three-dimensional nanostructures.

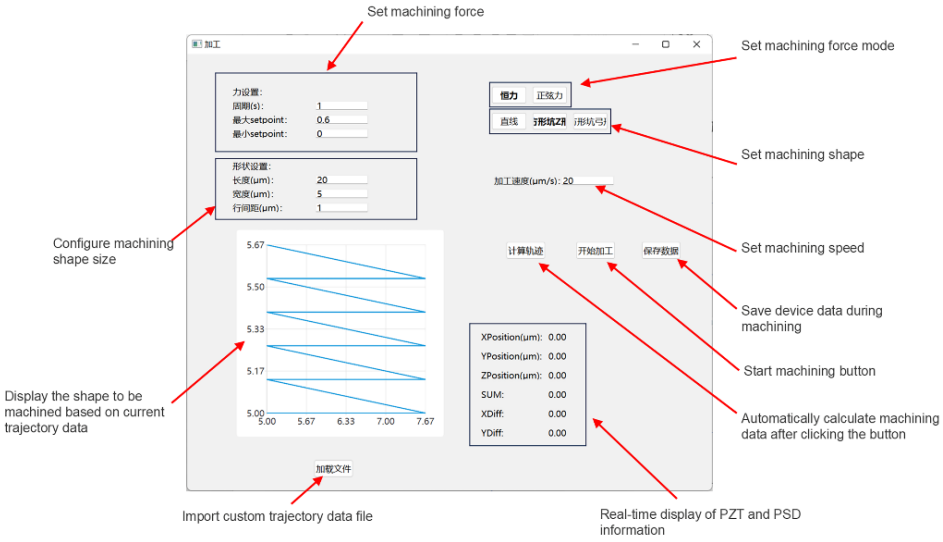

Figure 6. The interface of the machining module.

(4) Local surface detection module

The interface of the local surface detection module is shown in Figure 7. It primarily comprises the scanning image display area, the Trace and Retrace cross-sectional height graph display area, the scanning parameter configuration section, and the image parameter adjustment section, among others. The image display comprises two components: the scanned sample morphology image and the Error image. During localized detection, the XY-direction piezoelectric ceramics execute a fixed-period grating scanning motion. To facilitate real-time monitoring of the sample inspection status, one row of the scanning image is updated per scanning cycle, along with the corresponding Trace and Retrace cross-sectional height profiles for that cycle. The cross-sectional height profiles are displayed in real time, enabling users to adjust PID parameters and directly observe the sample inspection data. In the scanning parameter setting area, users can configure scanning parameters such as the scanning range and frequency.

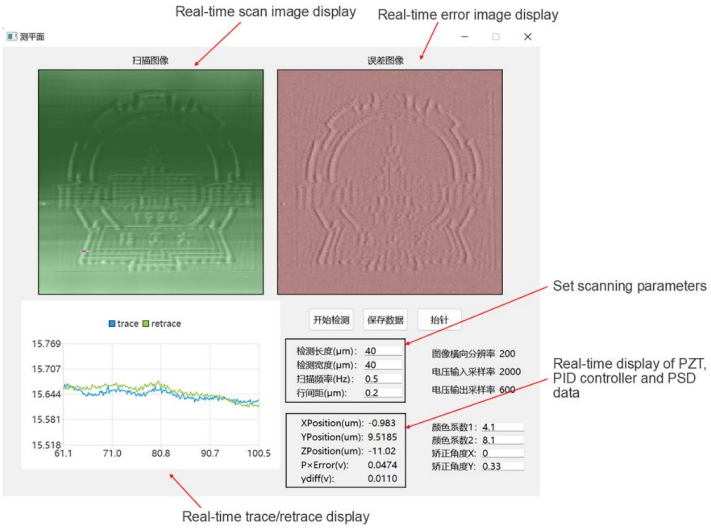

Figure 7. The interface of the machining module.

3. Results

3.1. Study on the method for centering the installation of microspheres

It is crucial to align the center of the microsphere with the center of the high-precision air-bearing rotary stage during machining and measurement. The piezoelectric stage of the AFM system has a limited expansion range of only 30 μm. If the eccentricity of the microsphere exceeds 15 μm at any position, rotating the turntable by 180 °would result in a positional discrepancy greater than 30 μm, surpassing the actuator's range. This can severely impact the detection and processing accuracy of the microsphere and potentially damage the probe and sample. Therefore, precise alignment of the microsphere's center is essential for effective machining. In this study, we employed CCD imaging with optical alignment software for coarse adjustment, followed by fine adjustment using a home-made AFM controlled by alignment software. The interface of the fine adjustment software is shown in Figure 8a.

The detailed procedure for the initial coarse adjustment is as follows: First, the microsphere is securely mounted on the two-dimensional manual displacement stage. The position of the CCD camera is then adjusted, and the focusing knob is rotated to ensure that the microsphere is clearly visible in the CCD field of view. Additionally, the high-precision air-bearing rotational stage is engaged to guarantee that the microsphere remains within the CCD's field of vision at all times. Then, the high-precision air float rotation stage is reset to zero and maintained at this position. The optical alignment software is initiated to capture the current position of the microsphere. Three equidistant points along the edge contour of the microsphere are selected to fit its outer contour, as shown in Figure 8b, and the coordinates of the center of the outer circle are recorded. Rotate the high-precision air float rotation axis by 180 °and maintain this position, as shown in Figure 8c. Reapply the optical aligning software to capture the current position of the microsphere, recording its outer circle outline and center coordinates in a manner consistent with the previous step. As shown in Figure 8d, the new center and outer circle profiles are calculated and fitted using optical aligning software based on the saved circle profiles and center parameters from the previous steps. At this point, the position of the circle's center corresponds to the position where the microsphere's center reattaches to the high-precision air-floating rotating stage. The position of the microsphere is adjusted by rotating the knob of the two-dimensional manual displacement table, ensuring that the actual profile of the microsphere in the CCD image precisely aligns with the fitted outer circular contour (Figure 8e). The coarse adjustment process is followed by fine adjustment to achieve precise alignment.

The detailed procedure for the precise adjustment is as follows: Move the probe to the initial contact position near the microsphere by controlling the electric displacement stage. Press the pin button to initiate the automatic approach of the probe towards the microsphere for contact. Press the start alignment button to initiate the alignment process. The system will begin displaying the relative position of the probe numerically. At this moment, the probe's position is designated as the reference point (relative position zero), and the initial extension position of the piezoelectric ceramic, which is closest to the ball, is recorded as x_0 (with the direction toward the ball defined as positive). The calculation method for determining the relative position of the probe during alignment is presented as follows:

$$r = h - a_0 * t - (x - x_0) \quad (9)$$

where r is the relative position of the probe during the alignment process. h is the vertical upward displacement distance of the electrically stage. a_0 is drop distance for each drop. x is the position of the piezoelectric stage and x_0 is the initial position of the piezoelectric stage, respectively.

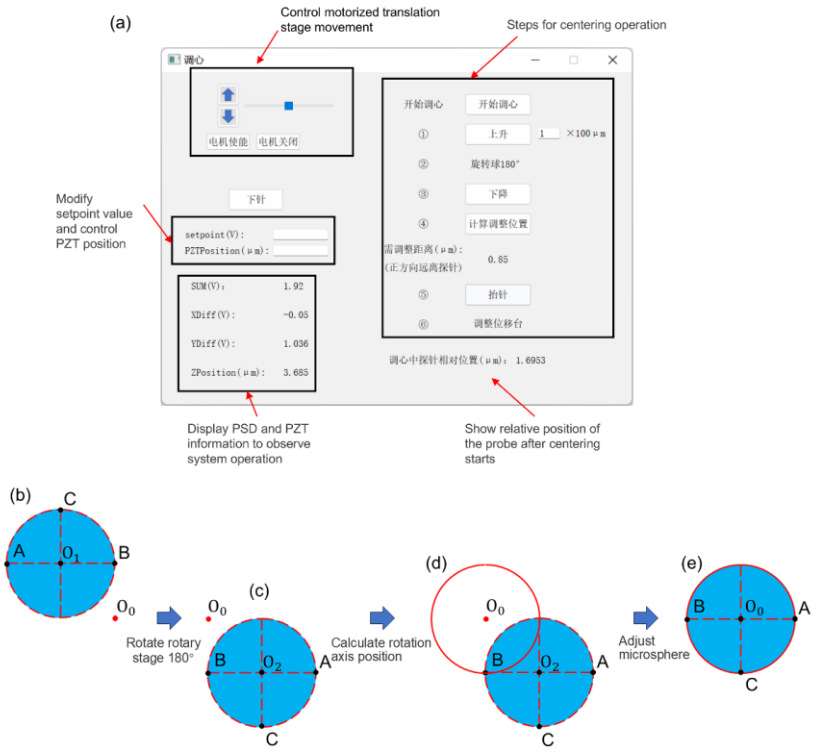

Figure 8. The software and process for centering the installation of microspheres. **(a)** The interface of the fine adjustment software; **(b–e)** The schematic diagram for the coarse adjustment process.

Point the rise button to send a specified number of fixed pulse signals to the stepper motor, causing it to move upward by a fixed distance denoted as h. This distance h represents the rise height, which can be adjusted based on the estimated degree of eccentricity. Rotate the ball through a 180-degree angle, then click the drop button to initiate the automatic engagement of the probe. The flow chart of this process is illustrated in Figure 4b. During the engagement, the electric displacement stage records the number of drops, denoted as t, and the drop distance for each drop is represented as a_0. Determine the position adjustment based on the coordinate changes of the probe before and after the elevation.

Press the probe lift button to prevent the probe from being struck during the adjustment of the manual stage. Adjust the position of the manual stage according to the distance indicated by the software display. Repeat this process until the calculated eccentricity is within 3 μm, at which point the fine adjustment in one direction is complete. Rotate the rotation stage by 90 degrees and repeat the aforementioned procedure, then conduct fine adjustments perpendicular to the previous orientation. Upon completing the adjustments in both perpendicular directions, all alignment operations will be finalized.

The diagram illustrating the alignment steps is presented in Figure 9, while the method for calculating the eccentric position is detailed as follows:

$$\mathrm{d} = (\mathrm{d}_1 - \mathrm{d}_2)/2 \tag{10}$$

where r is the distance that needs adjustment. d_1 and d_2 are the probe position at the initial point and second point of contact with the microsphere.

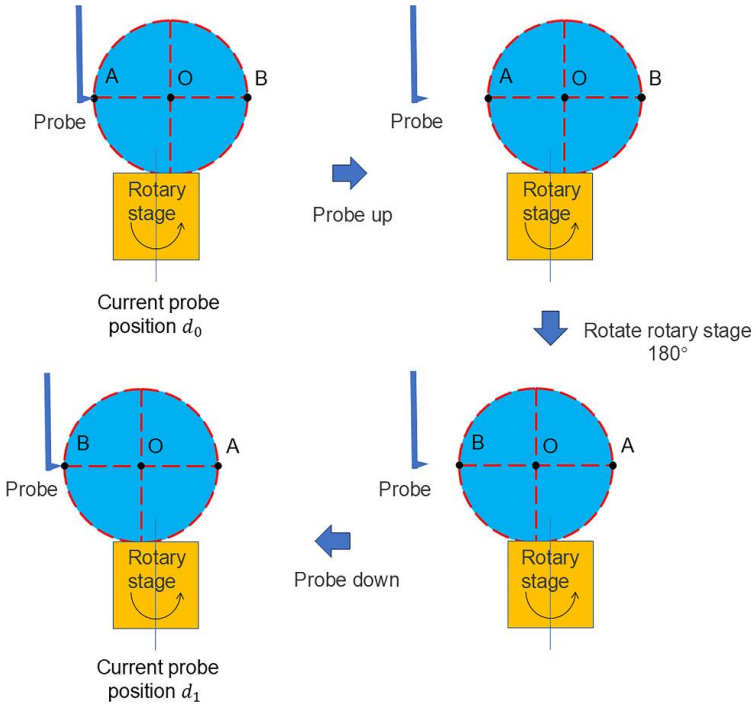

Figure 9. The schematic diagram of the precise alignment steps.

3.2. Machining and measurement on microspheres

To fully characterize the morphology of a sphere, theoretically, every point on its surface should be measured. However, due to the unique spatial structure of spheres, this is impractical in actual measurement scenarios. Two approximation methods are commonly employed: one involves measuring a portion of the spherical surface and using this local data to infer overall characteristics such as surface roughness. Instruments like atomic force microscopes (AFM), which offer high precision but have limited measurement ranges, are suitable for this approach. The second method entails measuring multiple circular profiles of the sphere and using these profiles to represent the overall geometry, such as assessing roundness and sphericity errors with a roundness meter. Given its high precision and minimal contact force, AFM is the preferred choice for measuring the surface topography of the target shot. Additionally, precision rotating stage and auxiliary indexing stage are essential for measuring the complete circumference of the target shot's surface in any orientation.

(1) Spherical circumferential trace measurement

In the experiment, GDP microspheres with a diameter of approximately 1500 μm were selected for circumferential trace detection, as illustrated in Figure 10a. The microsphere was securely affixed to the fixture, aligned carefully, and testing commenced following alignment. Multiple consecutive measurements were conducted at the same position on the microsphere, and the results were compared, as shown in Figure 10b. It is evident from the figure that numerous sharp peaks appear on the curve, which persist across multiple measurements. This indicates that there are indeed sharp points on the surface of the microsphere. Notably, the detection results from different measurement sessions exhibit

high consistency and correspond well, demonstrating that the equipment developed in this study can reliably perform circumferential trace detection with a good repeatability and that the system is stable.

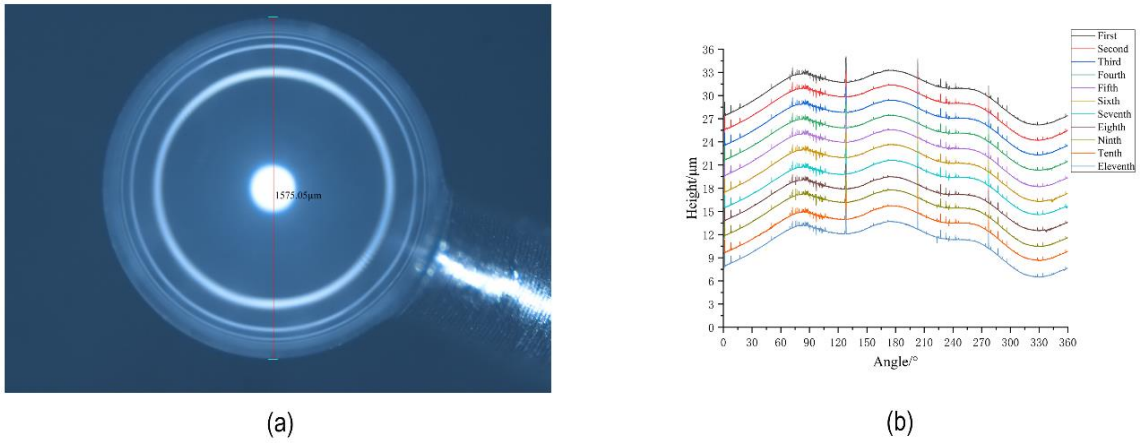

Figure 10. The results of spherical circumferential trace measurement. **(a)** The GDP miniaturized sphere; **(b)** The circular profile of the microsphere measured at the same position consistently.

(2) Micro-spherical machining and measurement

The home-made device was employed for the nano-machining on a microsphere. A diamond-coated AFM probe is selected in this study. By applying a normal load to the AFM tip, nanostructures were fabricated through the relative movement between the AFM tip and the microsphere surface. During the machining process, the air spindle remained stationary. After completing each structure, the spindle was rotated to the next designated machining position. In this study, we utilized this method to create square pits, circular pits, triangular pits, and nanogrooves at various locations on the microsphere surface. Figure 11 presents images of the nanostructures captured by the CCD in our home-made AFM system. As shown in the figure, square pits, circular pits, triangular pits, and nanogrooves were successfully fabricated on the microsphere surface.

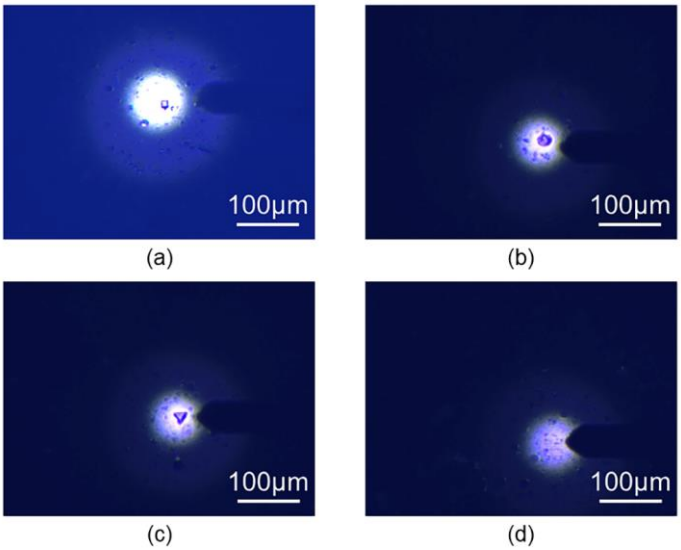

Figure 11. The nanostructures machined on microsphere surface: **(a)** Square pits (side length 10 μm); **(b)** Circular pits (side length 20 μm); **(c)** Triangular pits (side length 20 μm); **(d)** nanogrooves (length 30 μm).

After the machining process, the diamond-coated AFM probe was replaced with a measurement probe to examine the machined structure. The detection images obtained from the supporting software developed in this study are presented in Figure 12a–f. Figure 12a–c illustrate the 3D images reconstructed from the detection data. These 3D images clearly reveal the machined structure and spherical curvature. The machining and testing results demonstrate that the developed equipment is capable of achieving spherical machining and partial spherical surface measurement.

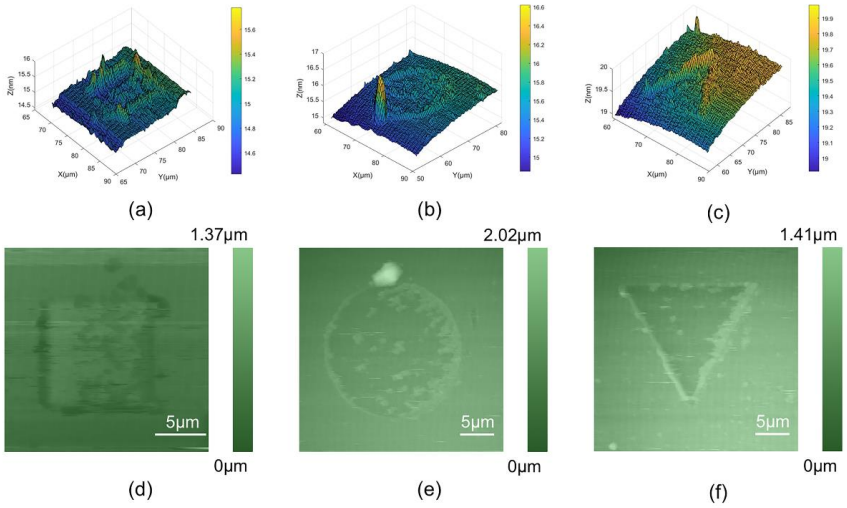

Figure 12. The 3D images of **(a)** Square pits, **(b)** Circular pits and **(c)** Triangular pits measured by home-made device. The corresponding 2D images of **(d)** Square pits, **(e)** Circular pits and **(f)** Triangular pits.

3.3. Performance evaluation of processing and testing of the integrated device

Previous study has been demonstrated that the processing position error resulting from the offset of the micro-ball center is more pronounced compared to the error motion of the air-bearing spindle. Furthermore, the processing position error resulting from the offset of the micro-ball center is less than 2.5 nm [7]. This indicates the integrated device has a good processing position accuracy. Hence, the probe wear and comparison of measurement results with standard systems are conducted in this section.

(1) Probe wear analysis

To evaluate the wear of the probe during the spherical circular trajectory detection performed by the device, a tip wear test experiment was carried out. The experiment employed a target ball with a diameter of 1300 μm as the sample and utilized the ContDLC probe manufactured by BudgetSensor Company, which has an elastic coefficient of 0.2 N/m. During the detection process, the cantilever deflection was approximately 200 nm, corresponding to a normal load of around 40 nN. Detection experiments were performed at the maximum circumference of the target ball for 5 cycles (approximately 20 mm), 10 cycles (approximately 40 mm), and 20 cycles (approximately 80 mm). The probes after detection were characterized using a scanning electron microscope (SEM), and the wear condition of the probes as well as their impact on the detection results were assessed based on the analysis of the target ball's surface morphology.

Figure 13a–d shows the SEM images of the new probe, the probe after 5 cycles of detection, the probe after 10 cycles of detection, and the probe after 20 cycles of detection, respectively. SEM analysis

revealed that the tip of the probe exhibited no significant wear. The experimental results demonstrate that, under an applied force of 40 nN, the probe exhibits minimal wear. This indicates that the developed AFM system induces negligible wear on the probe during spherical circular trajectory detection, thereby fulfilling the requirements for long-term measurements.

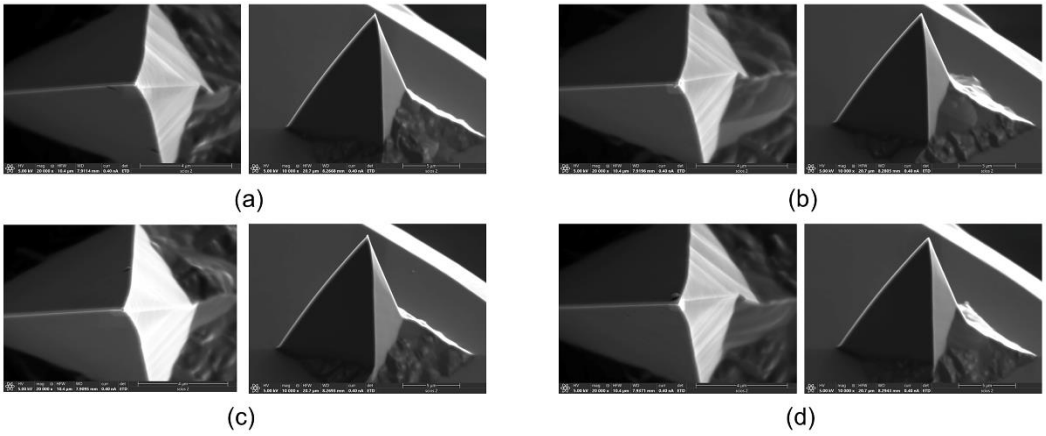

Figure 13. The SEM images of AFM tips: **(a)** Brind new tip; **(b)** Measured 5 circles; **(c)** Measured 10 circles; **(d)** Measured 20 circles.

(2) Comparison of measurement results with standard systems

To validate the detection performance of the device, the detection results obtained at various scanning frequencies were compared with those from a commercial atomic force microscope. A Z-shaped scanning trajectory was employed, and scanning experiments were performed at frequencies of 0.2 Hz, 0.4 Hz, 0.5 Hz, 0.6 Hz, 0.8 Hz, 1 Hz, 1.5 Hz, and 2 Hz. The experiments focused on the same region of TGF11, with a consistent scanning area of 40 μm × 15 μm. As shown in Figure 14, the scanning results obtained using the Z-shaped scanning trajectory at different scanning frequencies are presented. As shown in Figure 15, the cross-sectional height profiles of the home-made AFM at various scanning frequencies are compared with the profile obtained from the Bruker Dimension Icon AFM at 0.5 Hz. As shown in the two figures, under the low-frequency scanning range of 0.2–0.6 Hz, the Z-shaped scanning trajectory yields relatively clear images. The probe's movement along the X-axis is relatively stable, resulting in minimal image distortion. Compared to the detection results obtained from Bruker's atomic force microscope, the image quality of the home-made AFM at low scanning frequencies is comparable to the results achieved by Bruker's atomic force microscope at 0.5 Hz. During intermediate-frequency scanning in the range of 0.8–1 Hz, as the scanning speed increases, the detection results reveal that the bottom structure of the trapezoidal groove becomes increasingly distorted. When scanned at high frequencies ranging from 1.5 to 2 Hz, the detection image reveals significant distortion of the groove's bottom structure, rendering it nearly impossible to accurately measure the groove's bottom plane. Additionally, severe distortion is observed in the image at the points where the scanning direction reverses. Therefore, selecting a scanning frequency within the range of 0.2–0.6 Hz enables the achievement of detection results comparable to those obtained using the Dimension Icon AFM.

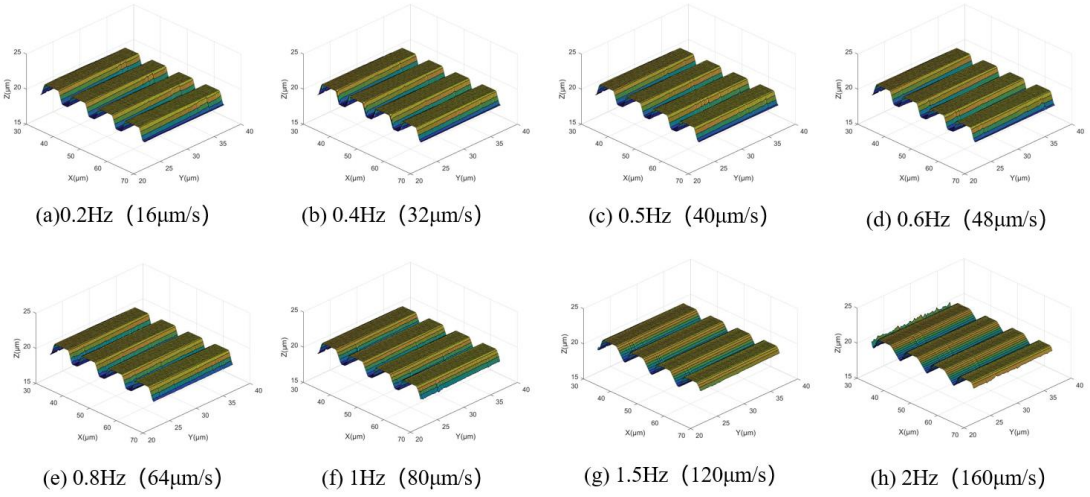

Figure 14. The AFM images of TGF11 sample obtained with different scanning frequences.

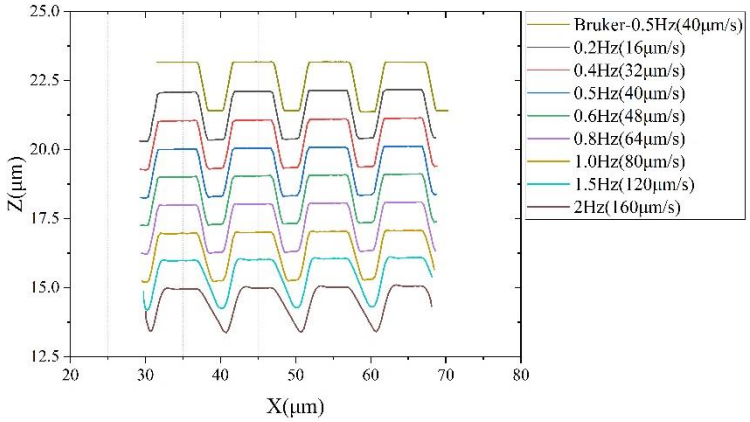

Figure 15. The comparison between the image cross-section measured by home-made device and commercial product.

4. Conclusion

An integrated device, comprising a homemade AFM system, a control system, and proprietary software, has been developed to achieve seamless integration of machining and measurement on the surface of microspheres. Moreover, the control system of the integrated device has also been established. The control system achieves closed-loop control of the analog quantity through a PID controller. Based on the C++ graphical user interface (GUI) application development framework Qt, the upper-computer software is developed, featuring four modules: a common function module, a sphere detection module, a machining module, and a local surface detection module. Furthermore, a strategy for aligning the rotating center of the microsphere with the air-bearing spindle is proposed, effectively addressing the challenge of center alignment in microsphere machining and testing. Finally, nanostructures, including square pit structures, triangular structures, and circular structures, are machined on the surface of a GDP microsphere with a diameter of approximately 1500 μm. The morphologies of these nanostructures were characterized by the device.

This study presents the independent development of an atomic force microscope system and achieves the integration of processing and detection on microspherical surfaces. Moreover, due to the

self-built nature of the device, it offers a wider range of motion adjustment and processing capability, enabling it to accommodate microspheres with larger diameters and thereby avoiding interference issues.

Acknowledgments

The authors gratefully acknowledge the financial supports of the National Natural Science Foundation of China (52405462, 52222512). Heilongjiang Provincial Postdoctoral Science Foundation (LBH–Z23171) and Postdoctoral Fellowship Program of CPSF (GZB20230952). China Postdoctoral Science Foundation (2023M740921) and Pre-research Task (NO. SKLRS202403B) of State Key Laboratory of Robotics and Systems (HIT).

Authors' contribution

Conceptualization, Jiqiang Wang, Yongda Yan and Yanquan Geng; methodology, Jiqiang Wang, Ziwen Kang, Yongda Yan and Yanquan Geng; software, Jiqiang Wang and Ziwen Kang; writing—original draft preparation, Jiqiang Wang and Ziwen Kang; writing—review and editing, Jiqiang Wang, Ziwen Kang, Yongda Yan and Yanquan Geng; funding acquisition, Jiqiang Wang and Yanquan Geng. All authors have read and agreed to the published version of the manuscript.

Conflicts of interests

The authors declare no conflict of interest.

References

[1] McEachern RL, Moore CE, Wallace RJ. The design, performance, and application of an atomic force microscope-based profilometer. *J. Vac. Sci. Technol. A* 1995, 13(3):983–989.

[2] Glendinning SG, Colvin J, Haan S, Kalantar DH, Landen OL, *et al.* Ablation front Rayleigh–Taylor growth experiments in spherically convergent geometry. *Phys. Plasma* 2000, 7(5):2033–2039.

[3] Carlson LC, Alfonso EL, Huang H, Nikroo A, Schoff ME. *et al.* Automation of NIF target characterization and laser ablation of domes using the 4pi system. *Fusion Sci. Technol.* 2015, 67(4):762–770.

[4] Takeuchi Y, Yoneyama Y, Ishida T, Kawai T. 6-axis control ultraprecision microgrooving on sculptured surfaces with non-rotational cutting tool. *CIRP Ann.* 2009, 58(1):53–56.

[5] Wang Y, Geng Y, Li G, Wang J, Fang Z, *et al.* Study of machining indentations over the entire surface of a target ball using the force modulation approach. *Int. J. Extreme Manuf.* 2021, 3(3):035102.

[6] Zhao X, Geng Y, Li W, Yan Y, Hu Z, *et al.* Fabrication and measurement of nanostructures on the micro ball surface using a modified atomic force microscope. *Rev. Sci. Instrum.* 2012, 83(11):115104.

[7] Geng Y, Wang Y, Yan Y, Zhao X. A novel AFM-based 5-axis nanoscale machine tool for fabrication of nanostructures on a micro ball. *Rev. Sci. Instrum.* 2017, 88(11):115109.

[8] K üng A, Meli F, Thalmann R. Ultraprecision micro-CMM using a low force 3D touch probe. *Meas. Sci. Technol.* 2007, 18(2):319.

[9] Zhao X. Sun T, Yan Y, Li Z, Dong S. Measurement of roundness and sphericity of the micro sphere based on atomic force microscope. *Key Eng. Mater.* 2006, 315–316:796–799.

[10] Chen L. Automatic 3D surface reconstruction and sphericity measurement of micro spherical balls of miniaturized coordinate measuring probes. *Meas. Sci. Technol.* 2007, 18(6):1748.

[11] Bartl G, Krystek M, Nicolaus A. PTB's enhanced stitching approach for the high-accuracy interferometric form error characterization of spheres. *Meas. Sci. Technol.* 2014, 25(6):064002.

[12] Bartl G, Krystek M, Nicolaus A, Giardini W. Interferometric determination of the topographies of absolute sphere radii using the sphere interferometer of PTB, *Meas. Sci. Technol.* 2010, 21(11):115101.

[13] Janecki D, Stępień K, Adamczak S. Sphericity measurements by the radial method: i. mathematical fundamentals. *Meas. Sci. Technol.* 2015, 27(1):015005.

[14] Lu B, Liu B, Sun H. Technology of target inspection by diffraction interferometer based on sub–aperture stitching. *High Power Laser Part. Beams* 2016, 28(2):022006.

[15] Zhao W, Li R, Duan L, Cheng Z, Pan Q, *et al.* High-precision radius and sphericity measurement for microspheres of micro-CMM probe tip. *Meas. Sci. Technol.* 2023, 34(10):105002.

[16] Oertel E, Manske E. Radius and roundness measurement of micro spheres based on a set of AFM surface scans. *Meas. Sci. Technol.* 2021, 32(4):044005.